carried out which coats carbon nanotubes with a C matrix. So the membrane can increase thermal stability, mechanical properties, and conductivity. The conductivity of the membrane composite was found to be 0.025 S/cm (El-Shahawy et al., 2022).

This research aims to improve the physical properties of the membrane and fill modified montmorillonite-carbon (MMT-Carbon) to reduce the matrix particle size in the phthalic anhydrous C matrix using the coprecipitation method. By reducing the particle size of CP by filling MMT-Carbon in nano form as a filler, it is strongly suspected that it can improve the performance characteristics of the membrane compared to C in general size.

## Experimental

### Material and Methods

The chitosan used in the matrix is C with a deacetylation degree of 88.83% and C that has been modified with phthalate anhydrate. The filler used is modified montmorillonite with carbon nanotubes (MMT-CNT). For membrane fabrication, 2% acetic acid, N,N-dimethylformamide, 1 M sodium hydroxide and 1 M sulfuric acid were used.

The equipment used in this research is a digital balance (Sartorius VB), spatula, bucket, stand and clamps, hot plate stirrer, magnetic stirrer, oven, Fourier Transform Infra Red Spectroscopy (FT-IR), X-Ray Diffraction (X-RD), Universal pH, thermometer, centrifugation device, funnel, 100 mesh sieve, and other glass equipment commonly used in laboratories.

### Procedures

### Membrane fabrication

The C matrix is made in 3 stages, namely deproteination, demineralization, and deacetylation. Meanwhile, for the chitosan-phthalate matrix, it is mixed between C and anhydrous phthalate with the solvent N,N-dimethylformamide (Chen et al., 2021). The filler used is MMT-CNT using the sol-gel method (Sanusi et al., 2021). Dissolve 2 grams of C powder in 80 mL of 2% acetic acid for 30 minutes. For the other beaker, fill it with 0.129 grams of filler dissolved in 10 mL of 2% acetic acid solution and stir for 30 minutes. The comparative composition is a 2% acetic acid solution then dispersed with various concentrations of C, CP, and MMT-Carbon respectively 2:0.05:0.129 grams, and sonicated for 30 minutes. In another beaker, dissolve 0.05 grams of phthalic anhydrous C in 10 mL of N, N-dimethylformamide while stirring for 30 minutes. Next, the two matrices were stirred for 30 minutes. After stirring for 30 minutes, filler was added and stirred for 30 minutes. The mixture is then placed onto a flat, clean acrylic plate. After the mixture was on the plate, it was dried at room temperature for 3 weeks. The membrane formed was soaked with 1 M sodium hydroxide for 15 minutes and then washed with distilled water until the pH was neutral. Next, the membrane was soaked in 1 M sulfuric acid solution for 24 hours. Then the membrane is pressed using a plastic plate and dried at room temperature until dry. The variations in membrane composition are made with the following compositions:

**Table 1.** Composition of materials for composite membrane fabrication.

| Membrane | Membrane type | Matrix | | Filler |
|---|---|---|---|---|
| | | (C) (grams) | (CP) (grams) | MMT-CNT (grams) |
| 1 | C 2,04 - CP 0.01/ MMT-CNT | 2.04 | 0.01 | 0.129 |
| 2 | C 2,02 - CP 0.03/ MMT-CNT | 2.02 | 0.03 | 0.129 |
| 3 | C 2,00 - CP 0.05/ MMT-CNT | 2.00 | 0.05 | 0.129 |
| 4 | C 1,98 - CP 0.07/ MMT-CNT | 1.98 | 0.07 | 0.129 |
| 5 | C 1,96 - CP 0.09/ MMT-CNT | 1.96 | 0.09 | 0.129 |

### Characterization

*FTIR***.** This analysis is used to analyze functional groups. The sample was mixed with 0.5 grams of KBr at room temperature. The two solids are mashed and mixed until homogeneous. Then the powder is pressed to form pellets. The analysis is in the wave number range of 400-4000 $cm^{-1}$.

*XRD*. XRD is used to analyze the level of crystallinity in the sample. A certain amount of sample is prepared in a dry pin tub holder. The analysis process was carried out with Cu-K α radiation (λ=0.154056 Å).

*SEM (Scanning Electron Microscopy)*. The membrane was analyzed using SEM to determine the morphological characteristics of the membrane. The membrane sheet is prepared on the pin stub holder. Then coating is carried out using gold. The analysis process is carried out at a certain magnification to get a clear surface image.

*Water uptake and Swelling of methanol*. The membrane was cut to size 2×2 cm, then dried in an oven, then weighed to obtain the dry weight of the membrane (Wdry). Then the membrane sample was soaked in 1 M water/methanol for 24 hours at room temperature. Then the membrane sample that had been soaked in 1 M water/methanol was weighed and the wet weight (Wwet) of the membrane was obtained. The absorption capacity for water/methanol is calculated using the equation:

$$\% \text{ Absorption capacity} = \frac{W_{wet} - W_{dry}}{\text{Membrane weight}} \times 100\% \quad (1)$$

*Ion exchange capacity*. Ion exchange capacity (IEC) is measured by the principle of acid-base titration. The membrane was cut into 2x2 cm pieces and soaked in 50 mL distilled water and placed in the oven at 60 °C for 1 hour, then 0.5 M HCl was added. The mixture was kept for 24 hours at room temperature. The solution taken was then titrated with 0.05 N NaOH with PP indicator. Calculation of IEC follows the following formula:

$$IEC = \frac{M\ NaOH \times V\ NaOH}{\text{Membrane weight}} \quad (2)$$

*Methanol Permeability*. Methanol permeability analysis was carried out using two compartments by filling 1 M methanol in compartment A and deionized water filling in compartment B. Between compartments A and B, a dry membrane was placed on a flat surface. Samples in compartment B were taken using a pipette every 30 minutes for 3 hours. The samples obtained were analyzed using a pycnometer. Methanol permeability can be calculated as the following equation:

$$P = \frac{S\ V_b\ L}{A\ C_{Ao}} \quad (3)$$

where P ($cm^2/s$) is the permeability of methanol solution, S is the slope of the methanol concentration curve against time in compartment B (water), Vb (mL) is the volume of compartment B (water), CAO (mol/L) is the initial concentration of methanol in compartment A (methanol), L (cm) membrane thickness, and A ($cm^2$) membrane area.

*Proton conductivity*. Proton conductivity analysis uses Electrochemical Impedance Spectroscopy (EIS) method where membrane proton conductivity is measured in a conductivity cell with Frequency Response Analysis. The analysis process covers a frequency range of 1-106 Hz and an amplitude of 0.01 A. Proton conductivity can be calculated according to the following equation:

$$\sigma = \frac{L}{AxR} \quad (4)$$

where σ ($S.cm^{-1}$) is proton conductivity, R (Ω) membrane resistance, A ($cm^2$) membrane surface area, and L (cm) membrane thickness.

*Membrane selectivity.* Membrane selectivity can be calculated based on the ratio of the proton conductivity and methanol permeability values. The calculation is based on the following equation:

$$\varphi = \frac{\sigma}{P} \quad (5)$$

where φ is membrane selectivity, σ ($S.cm^{-1}$) proton conductivity, and P ($cm^2/s$) methanol permeability.

*TGA (Thermo Gravimetric Analyzer).* The thermal stability of the composite mixture membrane was analyzed using thermogravimetry. The sample used is 2x2 cm in size. TGA analysis was analyzed at temperatures ranging from 25 to 800 °C under a nitrogen atmosphere, at a heating rate of 10 °C/min. In this thermal test, the glass transition (tg) is measured, namely the temperature at which the material changes from glass (solid) form to rubber form.

## Result and Discussion

### Characterization of traits

The membrane was characterized using FTIR to identify groups. FTIR spectra are shown in Figure 1. Membrane spectra show that there are almost the same functional groups in each membrane. In the C=O region wave numberis the amide I region. The C=O region wave number can be indicated due to the reaction of chitosan and silica which comes from MMT. This reaction takes the form of an electrostatic bond between the positively charged ammonium group from the chitosan backbone and the negatively charged SiOH. Apart from electrostatic bonds, there are also hydrogen bonds between the -SiOH group and the surface of multi-wave carbon nanotube (MW-CNT) and -OH or $-NH_2$ of chitosan (El-Shahawy et al., 2022). Apart from that, it is influenced by the addition of an increasing mass of chitosan phthalate.

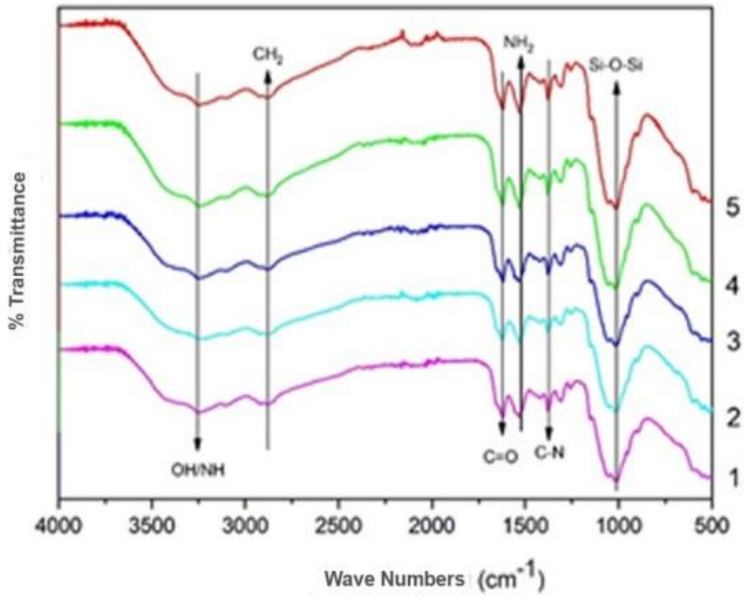


**Figure 1.** FTIR Spectra of Membrane (1). C 2.04 - CP 0.01/ MMT-CNT, (2). C 2.02 - CP 0.03/ MMT-CNT, (3). C 2.00 - CP 0.05/ MMT-CNT, (4). C 1.98 - CP 0.07/ MMT-CNT, (5). C 1.96 - CP 0.09/ MMT-CNT.

XRD diffractogram is used to determine the crystallinity of the composite membrane. Figure 2 shows the diffractogram of each membrane. The diffractogram results on each membrane have almost the same peaks. At 2θ = 20° represents the XRD pattern of C and CP. This peak experienced a decrease caused by an acylation reaction which destroyed hydrogen bonds involving the amine group of C (Sun et al., 2020). So this peak is a characteristic of CP. CP used in membrane fabrication increased from 0.01 grams to 0.09 grams. The peak 2θ = 10° shows the amorphous nature of the polymer. At this peak, the rigid crystal structure of chitosan is stabilized by intra- and intermolecular hydrogen bonds (X. Wang et al., 2021). Apart from that, the peak at 2θ = 10° also shows that there is an amorphous structure originating from the addition of CP. In addition, observations at 2θ = 26° indicate the presence of carbon atoms in the filler, namely MWCNTs. This can result in the sample being more amorphous.

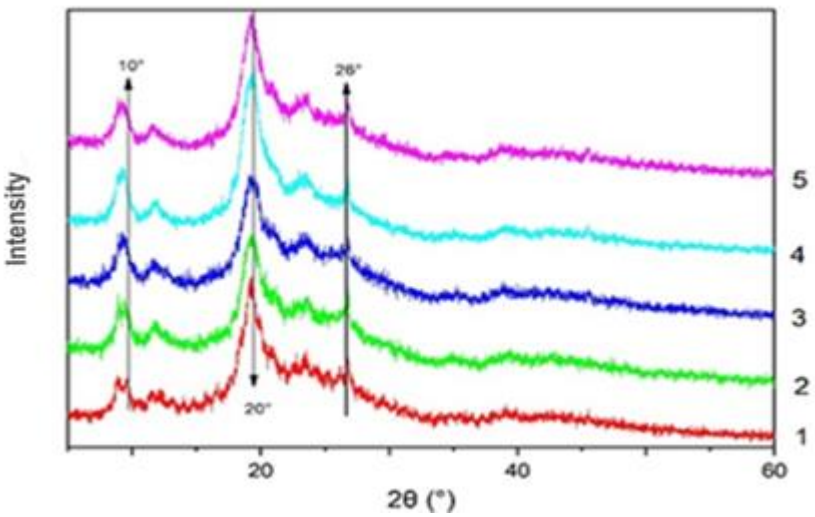


**Figure 2.** Membrane XRD diffractogram (1). C 2.04 - CP 0.01/ MMT-CNT, (2). C 2.02 - CP 0.03/ MMT-CNT, (3). C 2.00 - CP 0.05/ MMT-CNT, (4). C 1.98 - CP 0.07/ MMT-CNT, (5). C 1.96 - CP 0.09/ MMT-CNT.

Surface morphology analysis using SEM was carried out on CP Anhydrous and MMT-Carbon particles. The observed morphology is one or several Anhydrous CP and MMT-C particles taken randomly with a magnification of 10,000 times. A magnification of 10,000 times was used to observe the distribution of particles. The resulting Anhydrous CP and MMT-CNT show a nanoflake shape. Figure 3. This flake shape is in line with research conducted by (Ramimoghadam et al., 2013) which produced ZnO nanoparticles with flake morphology using the coprecipitation method. However, there are white lumps which are remnants of MMT that did not react with MWCNTs. The SEM results of the montmorillonite particles appear to have non-uniform sizes and tend to combine with each other. MMT-Carbon particles resulting from polysaccharide coprecipitation have the appearance of smaller particle size and a smoother surface. The use of this filler does not result in very significant cavities, so this indicates that there has been an interfacial interaction between the matrix and filler. It can also be concluded that the filler has a silica coating with hydrophilic properties which can increase the compatibility between the filler and the matrix. The mass of the chitosan matrix used decreased in mass from a to e, namely 2.04 grams to 1.96 grams, while the mass of the CP matrix increased from a to e by 0.01 grams to 0.09 grams. The addition of C can provide a smooth surface on the membrane. Apart from that, the interaction of C with CP causes agglomeration which produces fine pores (Spoială et al., 2021). The more CP used will produce pores on the membrane surface.

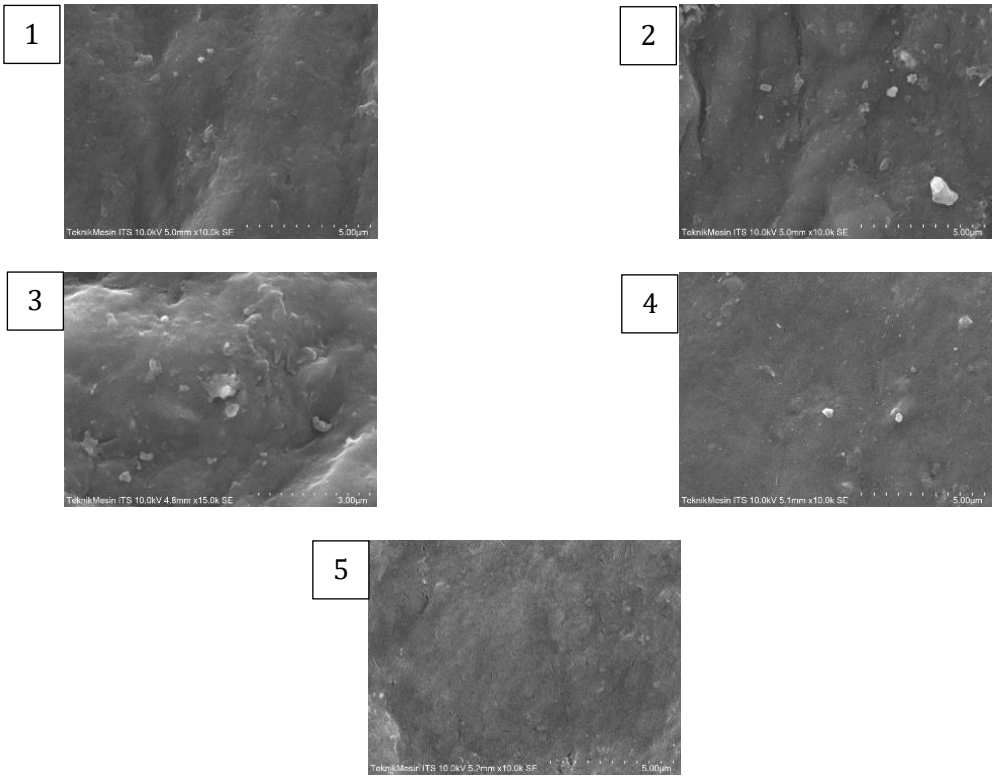


**Figure 3.** Membrane Surface Morphology (1). C 2.04 - CP 0.01/ MMT-CNT, (2). C 2.02 - CP 0.03/ MMT-CNT, (3). C 2.00 - CP 0.05/ MMT-CNT, (4). C 1.98 - CP 0.07/ MMT-CNT, (5). C 1.96 - CP 0.09/ MMT-CNT.

**Characterization of membrane performance**

The sweeping test functions to determine the amount of water absorbed by the membrane. According to the test results presented in Figure 4, it is stated that there is an effect of adding MMT-MWCNT filler to the phthalic anhydrous C matrix. Water absorption affects the transfer of negative ions which are converted into positive ions. If the water content in the membrane is sufficient for hydration then the speed of movement of positive ions through the membrane is the same as the speed of proton diffusion through water molecules. This can be interpreted that the proton conductivity is proportional to the content of water molecules in the membrane. Therefore, the higher the water content, the higher the proton conductivity and vice versa. However, the higher the water content will also affect the performance of the membrane, namely the water

swelling value on the membrane is too large, it will reduce the mechanical properties of the membrane, causing the membrane to become brittle. Seeing that the water content in the membrane really determines the conductivity of protons, controlling water in hydrogen cells requires special attention because water is produced continuously by reactions at the cathode (Zinola, 2022). Inorganic materials have high stability and hydrophilicity. This hydrophilic property can increase proton transfer from the anode to the cathode on the membrane (Xue et al., 2021). The results of the water swelling test are shown in Figure 4. The membranes that have the smallest water swelling are the 2nd membrane and the 5th membrane.

The methanol absorption capacity is shown in Figure 4. The methanol absorption capacity is the ability of the membrane to absorb methanol which is related to the methanol permeability. The high methanol absorption capacity means the methanol permeability is high. The absorption capacity of methanol influences ion transfer and the amount of methanol permeability (methanol cross over). This methanol cross over is also expected to have the smallest possible value. The presence of nanosilica MMT-o-MWCNTs which fills the pores in the phthalic anhydrous chitosan membrane matrix can inhibit the penetration of methanol into the membrane. The lowest methanol absorption capacity was owned by the 5th membrane with a composition of 1.96 g chitosan, 0.09 g phthalic anhydrous chitosan and 0.129 g MMT-MWCNT filler. High methanol absorption capacity is good for membranes, but the impact is also bad, there is methanol permeability, whereas membranes require low methanol permeability. The ability of the membrane to absorb methanol is influenced by the nature of the membrane polymer which has hydrophilic groups so that it is able to bind polar groups in methanol.

The IEC test results are shown in Figure 2. The membrane that has the largest IEC is the 2nd membrane. However, the optimal membrane taken is the 5th membrane which has strong mechanical properties because the membrane is not brittle, but also has good performance as a polymer electrolite membranes (PEM), namely having optimum water swelling and low methanol swelling.

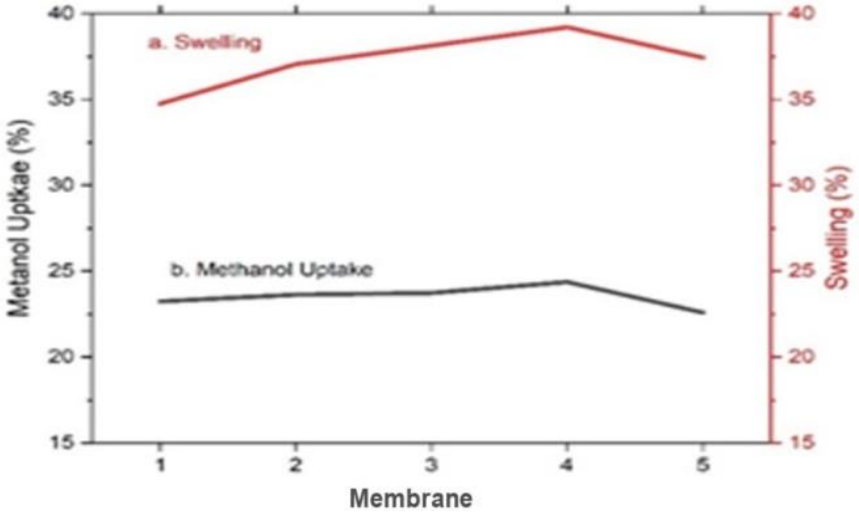


**Figure 4.** Graph (a). Swelling and (b). Methanol Uptake Membrane (1). C 2.04 - CP 0.01/ MMT-CNT, (2). C 2.02 - CP 0.03/ MMT-CNT, (3). C 2.00 - CP 0.05/ MMT-CNT, (4). K 1.98 - CP 0.07/ MMT-CNT, (5). C 1.96 - CP 0.09/ MMT-CNT.

A fuel cell requires a membrane that has optimum water swelling and low methanol absorption. Because water is a transport medium for H+ ions, if the water swelling is very low it will affect the transport of H+ ions, because water plays a role in the mobility of ion transport (Stenina & Yaroslavtsev, 2021). If the water swelling is large, the PEM will swell easily, thereby enlarging the pores and reducing the performance of the PEM as a separator between the anode and the cathode. Meanwhile, the IEC for the anhydrous phthalate chitosan-chitosan composite membrane as a result of this research was 0.74 meq/g. In PEM, a large IEC is needed, because the greater the IEC, the better the ability of the membrane to transmit protons from the anode to the cathode (Alaswad et al., 2021). Membranes for direct methanol fuel cell (DMFC) applications have high water swelling properties and low methanol swelling (Muhmed et al., 2021) because the proton transfer that occurs in the membrane occurs in the presence of water molecules in the membrane.

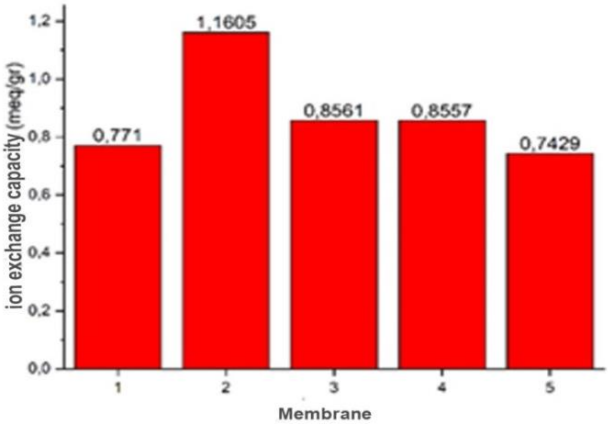


**Figure 5.** Ion Exchange Capacity Graph (Membrane (1). C 2.04 - CP 0.01/ MMT-CNT, (2). C 2.02 - CP 0.03/ MMT-CNT, (3). C 2.00 - CP 0.05/ MMT-CNT, (4). C 1.98 - CP 0.07/ MMT-CNT, (5). C 1.96 - CP 0.09/ MMT-CNT.

The results of methanol permeability, proton conductivity and membrane selectivity can be seen in Table 2. The results of methanol permeability fluctuate. This makes it possible for the collaboration of matrix and filler to have a certain level of composition. Each membrane has the ability to produce its own methanol permeability. The results of methanol permeability on the 5$^{th}$ membrane K 1.96 - KF 0.09/ MMT-CNT have the smallest value, namely 2.64 x $10^{-6}$ $cm^2/s$. The lowest methanol permeability value means that the least amount of methanol passes through the membrane surface every second. The low methanol permeability value is possible due to the use of the optimum filler MMT-o-MWCNTs of 0.129 grams. The use of this filler can prevent methanol from passing through the membrane because it has a large surface area so it can enter the matrix structure. In addition, the increasing use of CP matrix can lead to a change to a more nonpolar material. This is due to the presence of phthalate groups when matrix modification is carried out. Apart from that, CP can also reduce membrane porosity. Because the membrane pores can be blocked by the CP matrix. Apart from that, there are several membrane pores produced that are smaller than the methanol molecules, which means that methanol cannot pass through the membrane. The pores that methanol can pass through mean they have the same size or are larger than the methanol molecules. Besides that, the methanol permeability value of the C/CP membrane with montmorillonite modified with 3-aminopropyltriethoxysilane (Hanna Rosli et al., 2020) has a value of 0.36 x $10^{-5}$ $cm^2/S$. From these results it can be seen that modification with carbon nanotubes can reduce methanol permeability by 9.6 x $10^{-7}$ $cm^2/s$. This is possible because carbon nanotubes modified with montmorillonite can produce bonds that can reduce methanol permeability.

This bond comes from carboxylic acid from the walls of carbon nanotubes which have been oxidized with silica derived from montmorillonite. The results of the smallest permeability can be supported by observing the SEM image in Figure 3, which shows that there is little and good agglomeration.

**Table 2.** Membrane performance characterization results.

| Membrane | Permeability ($cm^2.s^{-1}$) | Proton Conductivity (S/cm) | Selectivity ($Ss/cm^3$) |
|---|---|---|---|
| 1 | 8.92x$10^{-6}$ | 1.984x$10^{-7}$ | 0.022247 |
| 2 | 3.95x$10^{-6}$ | 6.164x$10^{-7}$ | 0.156100 |
| 3 | 8.05x$10^{-6}$ | 8.361x$10^{-7}$ | 0.103860 |
| 4 | 8.66x$10^{-6}$ | 1.826x$10^{-6}$ | 0.210750 |
| 5 | 2.64x$10^{-6}$ | 3.352x$10^{-6}$ | 1.271400 |

The results of proton conductivity are used to determine the ability of a membrane to allow protons to pass through. The results of membrane conductivity measurements can be seen in Table 1. It can be seen that the highest

conductivity was obtained on the 5th membrane K 1.96 - KF 0.09/ MMT-CNT at 3.352 x $10^{-6}$ S/cm. Apart from that, research results (Tellez-Cruz et al., 2021) show that the C/C membrane with montmorillonite modified with 3-aminopropyltriethoxysilane has a conductivity value of 9.41 x $10^{-3}$ S/cm. According to (Tohidian & Ghaffarian, 2021) chitosan membranes with carbon nanotubes can provide a proton conductivity value of 4.4 x $10^{-2}$ S/cm. The addition of carbon nanotubes can influence the results of higher proton conductivity due to the interaction of $SO^{3-}$ from carbon nanotubes and $NH_2$ from chitosan. The decrease in proton conductivity is possible due to a decrease in the number of ionic groups. One of the functions of ionic groups is to serve as a pathway for protons. Each membrane has the same amount of filler. By using this filler, dispersion occurs between the chitosan and the filler and electrostatic interactions and hydrogen bond interactions occur (Huang et al., 2020). This interaction can form a continuous proton transport channel in the composite membrane.

The addition of CP can provide higher conductivity. This is possible because of the presence of polar groups in chitosan/anhydrous phthalate. This group can give rise to or create hydrophilic areas on the membrane because of its strong affinity for water. The hydrophilic region in the ion chain group can cause large water absorption which can be used for proton conduction using a hopping mechanism (Zhang et al., 2022). The hopping mechanism can be called the grottus mechanism. In this mechanism, protons move by jumping from proton sites in the closest range to other sites with the help of a network of hydrogen bonds in the membrane structure. The movement of protons is assisted by $NH^{3+}$ and $SO^{3-}$ ions. This factor causes membrane conductivity to increase (Duan et al., 2022).

Large water absorption can act as an active hydrophilic site and form ionic groups through hydrogen bonds. However, the use of more CP may inhibit proton transfer due to interfacial boundary effects. So it can interfere with the hydrophilic channel and will inhibit the proton channel. From the two membrane capabilities, namely high proton conductivity and low methanol permeability, the membrane selectivity parameters are obtained. A high selectivity value will produce better performance which is used as an indicator of the suitability of membranes used for DMFC applications. Membrane selectivity is obtained from the ratio of proton conductivity to methanol permeability.

The 5th membrane C 1.96 - CP 0.09/ MMT-CNT has the lowest methanol permeability value, has the highest proton conductivity value, and produces the highest membrane selectivity, namely 1.2714 Ss/$cm^3$. The membrane has a composition of 1.96 grams of C, 0.09 grams of CP, and 0.129 grams of MMT-o-MWCNTs filler. The difference in selectivity is influenced by the value of proton conductivity and methanol permeability. The matrix and filler used can support its ability as a DMFC electrolyte membrane. The addition of the most CP can affect the membrane working system. So this membrane can be used as an electrolyte membrane for DMFC applications by paying attention to the optimum composition when fabricating the membrane.

Characterization using TGA (Thermogravimetric Analysis) on the membrane aims to determine the stability and thermal decomposition behavior of the components that make up the membrane. In this research, TGA analysis was carried out on membranes that had good water and methanol absorption values and high IEC values. Based on water and methanol absorption data and IEC, the 5th membrane was selected for thermal analysis using TGA. The TGA thermogram and the percentage of total mass lost from the C-CP/MMT-CNT composite membrane on the 5th membrane are shown in Figure 6.

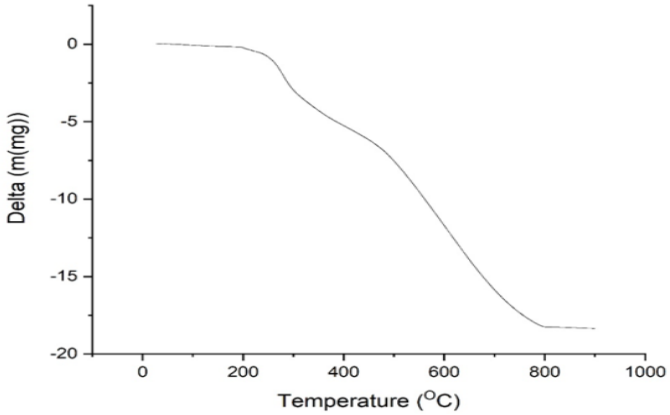


**Figure 6.** 5th Membrane TGA Curve C 1.96 - CP 0.09/ MMT-CNT.

Figure 6 shows that the C-CP/MMT-MWCNT composite membrane experienced 3 stages of thermal decomposition. The first stage of thermal decomposition occurs at a temperature of 160-200 °C which indicates the evaporation of water molecules in the membrane. The second stage of thermal decomposition occurred at a temperature of 290-300 °C which showed degradation of the chitosan bond with silane on the membrane and degradation of the C bond with the MMT-MWCNT surface. At this stage, the C-CP/MMT-CNT membrane had the lowest mass percentage reduction. This shows that the C-CP/MMT-CNT membrane has better thermal stability. The final stage of thermal decomposition takes place at a temperature of 490-790 °C where at this stage the decomposition of the remaining organic groups and degradation of the C polymer chain occurs. From the 3 stages of the thermal decomposition process of the membrane, it can be concluded that the C-CP/MMT-CNT membrane is stable up to 290 °C, which is far above the normal operating temperature of DMFC. All composite blend membranes showed better thermal stability than Nafion-117 membranes as well as base polymers. The results show that the thermal stability of the C-CP/MMT-CNT membrane is high enough to meet the requirements of DMFC.

## Conclusion

Membrane characterization using FTIR which shows the same functional groups, XRD diffractogram which shows almost the same crystallinity, and SEM analysis shows that the membrane with C 1.96-CP 0.09/ MMT-CNT has a smoother surface compared to the other compositions. Apart from that, membrane performance was also characterized, namely methanol permeability and proton conductivity. The lowest methanol permeability results were found in the 5$^{th}$ membrane K 1.96-KF 0.09/ MMT-CNT with a result of 2.64x10$^{-6}$ cm$^2$/s which was supported by the lowest methanol uptake. Meanwhile, the highest proton conductivity results were found in the 5$^{th}$ K 1.96 - KF 0.09/ MMT-CNT membrane of 3.352x10$^{-6}$ S/cm which was supported by swelling and ion exchange capacity. From the results of these two characterizations, it was found that the highest selectivity for the 5$^{th}$ membrane C 1.96-CP 0.09/ MMT-CNT was 1.2714 Ss/cm$^3$ and membrane stability at a temperature of 290 °C. Thus, the optimum matrix composition is 1.96 grams of C, 0.09 grams of CP, and 0.129 grams of filler.

## Conflict of Interest

The authors declare that there is no conflict of interest.

## References

Aburabie, J., Lalia, B., & Hashaikeh, R. (2021). Proton conductive, low methanol crossover cellulose-based membranes. *Membranes*, 11(7), 1–15. https://doi.org/10.3390/membranes11070539

Alaswad, A., Omran, A., Sodre, J. R., Wilberforce, T., Pignatelli, G., Dassisti, M., Baroutaji, A., & Olabi, A. G. (2021). Technical and Commercial Challenges of Proton-Exchange Membrane (PEM) Fuel Cells. *Energies*, 14(1), 1–21. https://doi.org/10.3390/en14010144

Chen, W. P., Huang, D. J., Hu, Z., Zhuang, Y. L., & Lu, S. T. (2021). Preparation and characterization of 6-O-caffeic acid chitosan. *Journal of Physics: Conference Series*, 1765(1), 1–7. https://doi.org/10.1088/1742-6596/1765/1/012029

Duan, Y., Ru, C., & Li, J. (2022). *Enhancing proton conductivity and methanol resistance of SPAEK membrane by incorporating MOF with flexible alkyl sulfonic acid for DMFC*. *641*(January).

El-Shahawy, A. A. G., Elnagar, N., Zohery, M., Abd Elhafeez, M. S., & El-Dek, S. I. (2022). Smart nanocarrier-based chitosan @silica coated carbon nanotubes composite for breast cancer treatment approach. *International Journal of Polymeric Materials and Polymeric Biomaterials*, 71(12), 910–922. https://doi.org/10.1080/00914037.2021.1925277

Hanna Rosli, N. A., Loh, K. S., Wong, W. Y., Mohamad Yunus, R., Khoon Lee, T., Ahmad, A., & Chong, S. T. (2020). Review of chitosan-based polymers as proton exchange membranes and roles of chitosan-supported ionic liquids. *International Journal of Molecular Sciences*, 21(2), 2–52. https://doi.org/10.3390/ijms21020632

Huang, D., Zheng, Y., Zhang, Z., Quan, Q., & Qiang, X. (2020). Synergistic effect of hydrophilic palygorskite and hydrophobic zein particles on the properties of chitosan films. *Materials and Design*, 185, 108229. https://doi.org/10.1016/j.matdes.2019.108229

Muhmed, S. A., Jaafar, J., Daud, S. S., Hanifah, M. F. R., Purwanto, M., Othman, M. H. D., Rahman, M. A., & Ismail, A. F. (2021). Improvement in properties of nanocrystalline cellulose/poly (vinylidene fluoride) nanocomposite membrane for direct methanol fuel cell application. *Journal of Environmental Chemical Engineering*, 9(4), 105577. https://doi.org/10.1016/j.jece.2021.105577

Ramimoghadam, D., Bin Hussein, M. Z., & Taufiq-Yap, Y. H. (2013). Hydrothermal synthesis of zinc oxide nanoparticles using rice as soft biotemplate. *Chemistry Central Journal*, 7(1), 1–10. https://doi.org/10.1186/1752-153X-7-136

Sanusi, O. M., Benelfellah, A., Papadopoulos, L., Terzopoulou, Z., Malletzidou, L., Vasileiadis, I. G., Chrissafis, K., Bikiaris, D. N., & Aït Hocine, N. (2021). Influence of montmorillonite/carbon nanotube

hybrid nanofillers on the properties of poly(lactic acid). *Applied Clay Science*, 201(November), 105925. https://doi.org/10.1016/j.clay.2020.105925

Spoială, A., Ilie, C. I., Ficai, D., Ficai, A., & Andronescu, E. (2021). Chitosan-based nanocomposite polymeric membranes for water purification—a review. *Materials*, 14(9), 1–29. https://doi.org/10.3390/ma14092091

Stenina, I. A., & Yaroslavtsev, A. B. (2021). Ionic mobility in ion-exchange membranes. *Membranes*, 11(3), 1–20. https://doi.org/10.3390/membranes11030198

Sun, M., Yuan, L., Yang, X., & Shao, L. (2020). Preparation and Modification of Chitosan-based Membrane. *ES Materials & Manufacturing*, 40–47.

Tellez-Cruz, M. M., Escorihuela, J., Solorza-Feria, O., & Compañ, V. (2021). Proton exchange membrane fuel cells (Pemfcs): Advances and challenges. *Polymers*, 13(18), 1–54. https://doi.org/10.3390/polym13183064

Tohidian, M., & Ghaffarian, S. R. (2021). Polyelectrolyte nanocomposite membranes based on chitosan and surface modified multi-walled carbon nanotubes for use in fuel cell applications. *Journal of Macromolecular Science, Part A: Pure and Applied Chemistry*, 58(11), 778–791. https://doi.org/10.1080/10601325.2021.1944200

Wang, W., Xue, C., & Mao, X. (2020). Chitosan: Structural modification, biological activity and application. *International Journal of Biological Macromolecules*, 164, 4532–4546. https://doi.org/10.1016/j.ijbiomac.2020.09.042

Wang, X., Zhou, P., Lv, X., & Liang, Y. (2021). Insight into the structure-function relationships of the solubility of chitin/chitosan in natural deep eutectic solvents. *Materials Today Communications*, 27(April), 102374. https://doi.org/10.1016/j.mtcomm.2021.102374

Xue, Q., Yang, D. J., Wang, J., Li, B., Ming, P. W., & Zhang, C. M. (2021). Enhanced mass transfer and proton conduction of cathode catalyst layer for proton exchange membrane fuel cell through filling polyhedral oligomeric silsesquioxane. *Journal of Power Sources*, 487(August 2020), 229413. https://doi.org/10.1016/j.jpowsour.2020.229413

Zhang, L., Liu, Z., Yang, C., García Sakai, V., Tyagi, M., & Hong, L. (2022). Conduction Mechanism in Graphene Oxide Membranes with Varied Water Content: From Proton Hopping Dominant to Ion Diffusion Dominant. *ACS Nano*, 16(9), 13771–13782. https://doi.org/10.1021/acsnano.2c00686

Zinola, C. F. (2022). Theoretical description and experimental characterization of water content distributions in hydrogen PEM fuel cells. *Chemical Engineering Journal*, 435, 1–35. https://doi.org/10.1016/j.cej.2022.134767